Competing stripe and magnetic phases in the cuprates from first principles

Yubo Zhang[a], Christopher Lane[b], James W. Furness[a], Bernardo Barbiellini[c,b], John P. Perdew[d,e,1], Robert S. Markiewicz[b], Arun Bansil[b,1], and Jianwei Sun[a,1]

[a]Department of Physics and Engineering Physics, Tulane University, New Orleans, LA 70118; [b]Department of Physics, Northeastern University, Boston, MA 02115; [c]Department of Physics, School of Engineering Science, LUT University, FI-53851 Lappeenranta, Finland; [d]Department of Physics, Temple University, Philadelphia, PA 19122; and [e]Department of Chemistry, Temple University, Philadelphia, PA 19122

Contributed by John P. Perdew, November 8, 2019 (sent for review June 26, 2019; reviewed by E. W. Plummer and Xinguo Ren)

Realistic description of competing phases in complex quantum materials has proven extremely challenging. For example, much of the existing density-functional-theory-based first-principles framework fails in the cuprate superconductors. Various many-body approaches involve generic model Hamiltonians and do not account for the interplay between the spin, charge, and lattice degrees of freedom. Here, by deploying the recently constructed strongly constrained and appropriately normed (SCAN) density functional, we show how the landscape of competing stripe and magnetic phases can be addressed on a first-principles basis both in the parent insulator $YBa_2Cu_3O_6$ and the near-optimally doped $YBa_2Cu_3O_7$ as archetype cuprate compounds. In $YBa_2Cu_3O_7$, we find many stripe phases that are nearly degenerate with the ground state and may give rise to the pseudogap state from which the high-temperature superconducting state emerges. We invoke no free parameters such as the Hubbard *U*, which has been the basis of much of the existing cuprate literature. Lattice degrees of freedom are found to be crucially important in stabilizing the various phases.

cuprates | stripes | density functional theory | high-temperature superconductivity | first principles

Competing orders lie at the heart of myriad fascinating properties of complex materials and their evolution with external controls of temperature, pressure, doping, and magnetic field (1). The parent compounds of the cuprate high-temperature superconducting materials, for example, are antiferromagnetic (AFM) insulators, which become high-temperature superconductors when doped with holes or electrons. This insulator–superconductor transformation is very complex and involves the presence of intervening pseudogap (2–6) and stripe (7) phases and mysterious mechanisms for arresting superconductivity with increasing doping, so that the superconducting phase occupies a characteristic dome-shaped region (8) in the phase diagram. Similarly, a wide variety of orders and the associated phase diagrams are exhibited by iron-based superconductors, heavy-fermion compounds, organics, and iridates, among other correlated materials of current interest (1, 9–11).

Complex materials, which often involve strong electronic correlations, present a challenge to first-principles approaches. The local spin density and the generalized-gradient approximations used commonly within the first-principles density functional theory (DFT) framework yield a metallic rather than the experimentally observed insulating AFM ground state in undoped cuprates (12, 13), so that a meaningful treatment of doping-dependent electronic structures of the cuprates on this basis becomes impossible. The AFM state can be stabilized by invoking an ad hoc Hubbard *U* parameter in a DFT+*U* approach (14, 15), but that limits the predictive power of the theory. An alternate route is to deploy effective model Hamiltonians (such as the Hubbard Hamiltonian with an explicit on-site Coulomb repulsion between electrons) and attempt an exact treatment of this model using quantum Monte Carlo (QMC) and other techniques (16, 17). However, in view of their heavy computational cost, such studies have been limited to fairly small clusters and 1-band, or at most 3-band, models of the cuprates and cannot be material-specific or allow modifications in the Hamiltonian in response to interactions between the charge, spin, and lattice degrees of freedom in the system.

There has been recent progress in the construction of advanced density functionals by satisfying many mathematical properties of the exact density functional. This progress offers a new pathway for addressing at the first-principles level the electronic structures of correlated materials. In particular, the strongly constrained and appropriately normed (SCAN) functional (18, 19), which satisfies 17 exact constraints, has been shown to provide a viable parameter-free description of diverse kinds of bonding environments (19–24), including the half-filled AFM ground state of the cuprates and their transition from the insulator to the metallic state with doping (*SI Appendix*, section 1) (12). In La_2CuO_4, one correctly captures in this way the size of the optical band gap (25–28), the value of the copper magnetic moment and its alignment in the cuprate plane (29), and the magnetic form factor in good accord with the corresponding experimental results. Because the SCAN approximation is implemented in a generalized Kohn–Sham scheme, the gap in its

Significance

High-temperature superconductivity, first discovered in materials with copper-oxide planes, is still not well understood. Cuprates exhibit complex phase diagrams under temperature and doping and have not been amenable to first-principles description using previous density functionals, but the recent SCAN functional correctly predicts many properties of the undoped and doped YBCO compounds. In the oxygen-doped $YBa_2Cu_3O_7$, SCAN finds many competing states with charge and spin stripes. Thermal energies will mix these states, creating fluctuations of the spin moments on the copper atoms in the pseudogap phase from which superconductivity emerges. Our study suggests a paradigm in which the physics of the mysterious pseudogap phase in the cuprates is encoded through a landscape of underlying competing phases in the material.

Author contributions: B.B., J.P.P., R.S.M., A.B., and J.S. designed research; Y.Z., C.L., and J.W.F. performed research; Y.Z., C.L., J.W.F., B.B., J.P.P., R.S.M., A.B., and J.S. analyzed data; and Y.Z., C.L., J.W.F., B.B., J.P.P., R.S.M., A.B., and J.S. wrote the paper.

Reviewers: E.W.P., Louisiana State University; and X.R., University of Science and Technology of China.

Competing interest statement: E.W.P. is an unpaid Advisory Board member for the Energy Frontier Research Center "Center for Complex Materials from First Principles," which supported the work of several of the authors.

[1]To whom correspondence may be addressed. Email: perdew@temple.edu, ar.bansil@northeastern.edu, or jsun@tulane.edu.

This article contains supporting information online at https://www.pnas.org/lookup/suppl/doi:10.1073/pnas.1910411116/-/DCSupplemental.

1-electron spectrum equals (30) the associated fundamental gap, defined as the energy difference, $E_{N-1} + E_{N+1} - 2E_N$, where the subscripts N, $N+1$, and $N-1$ denote ground-state energies of the N and $N \pm 1$ electron system (13) (*SI Appendix*, sections 2 and 3).

Here, we discuss energies and other characteristics of magnetic and stripe phases in $YBa_2Cu_3O_6$ ($YBCO_6$) and $YBa_2Cu_3O_7$ ($YBCO_7$), as exemplar cuprate compounds, using SCAN-based DFT computations. $YBCO_6$ is representative of the parent insulating compounds, while $YBCO_7$ lies deep within the superconducting dome around the optimally doped region in the phase diagram. No material-specific free parameter is involved. In particular, the Hubbard U parameter is not invoked. All computations have been carried out to a high degree of self-consistency and provide evidence for interactions between the spin, charge, and lattice degrees of freedom. We identify 20 distinct stripe phases in $YBCO_7$ and 6 in $YBCO_6$. The ground state in $YBCO_6$ is found to be reasonably well separated from the nearest competing energy state by ~10 meV/planar-Cu (~kT for $T = 120$ K). In sharp contrast, in $YBCO_7$, a large number of states are found to be nearly degenerate with the ground state. All stripe phases in $YBCO_7$ ($YBCO_6$) carry persistent copper magnetic moments of about 0.4 (0.5) μ_B/Cu. Lattice degrees of freedom play a key role in stabilizing the stripe phases, and the self-consistency process between the various degrees of freedom induces substantial changes in stripe periodicity and the spin and charge distributions.

A stripe state is a special combination of spin and charge distribution in which domains of approximately (π, π) AFM order are separated by antiphase boundaries (APBs), where magnetic moments are suppressed and charge densities are enhanced (1–4, 16, 17, 31, 32). Fig. 1*A* shows a schematic 1-dimensional (1D) stripe with 3-unit width, where a unit refers to a CuO_2 square or, equivalently, a Cu atom. The charge density in this stripe has a periodicity of $P_c = 3$; the spin density or magnetism also has a periodicity of $P_m = 3$. This is a so-called bond-centered stripe because the APB passes through the center of the Cu–Cu bonds. The central portion of the figure contains excess charge density (indicated by the large size of the green filled circles) and thus constitutes a charge stripe. In contrast, the outer portions of the figure contain excess spin density (indicated by large pink arrows) and form a magnetic stripe. Fig. 1*B* shows a schematic of a stripe of $P_c = 4$, but now the magnetic periodicity is $P_m = 8$. Note that this is a site-centered stripe since the APB now passes through the Cu sites. Due to the presence of the APB, $P_m = 2P_c$ for even values of P_c, but when P_c is odd, $P_m = P_c$.

Fig. 1*C* illustrates the interplay between the spin, charge, and lattice degrees of freedom by considering details of a 1D bond-centered stripe ($P_c = 4$) in $YBCO_7$. Stripe formation results in a modulation of hole doping on the planar oxygen atoms, as seen from the filled green circles in Fig. 1*C*, *Bottom*, with a clear excess of holes in the region of charge stripes where magnetism is reduced or suppressed. In contrast, hole doping on Cu (blue filled squares) is larger on the magnetic stripes and acts to compensate the oxygen holes. Note that the charge modulation is relatively small, ±0.02 holes on oxygen and ±0.005 holes on copper, while the average doping is 0.21. These small modulations are consistent with the results of ref. 36, where very small charge transfer (inconsistent with formal valence arguments) was reported. Lattice distortions are particularly prominent around the APBs, as we would expect. The black arrows in Fig. 1*C* show that the main deformation involves the movement of oxygen atoms toward the APBs with amplitudes of ~0.02 Å; see *SI Appendix*, section 6 for details. This results in a distortion of the structure with the appearance of a breathing mode. The fact that stripes can be seen with X-rays (37) indicates that there must be significant lattice distortions, although the precise atomic displacements involved in the stripe patterns are currently unknown.

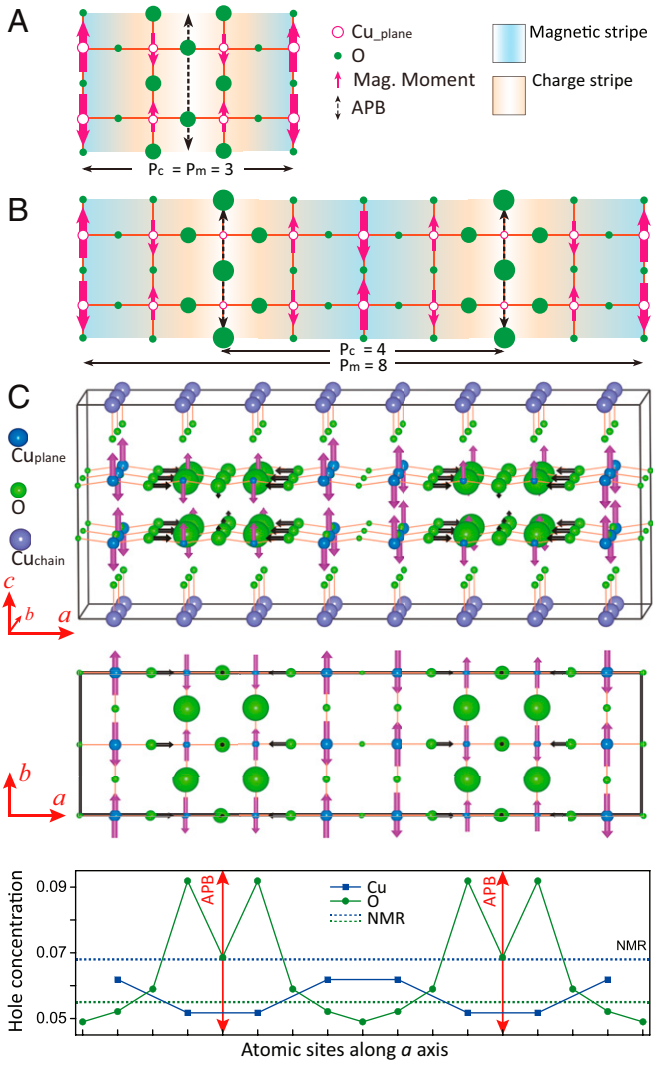

Fig. 1. Schematics of bond- and site-centered stripes and details of a representative self-consistently computed stripe structure in $YBCO_7$. (*A*) Schematic of a bond-centered stripe in which the APB passes through oxygen atoms (green dots) that lie in between copper (red circles) atoms; $P_c = P_m = 3$, where P_c and P_m denote periodicities (in terms of the number of Cu atoms or CuO_2 squares) of the charge and spin densities, respectively. (*B*) Schematic of a site-centered stripe in which the APB passes through copper atoms with $P_c = 4$ and $P_m = 8$. (*C*) A 1D bond-centered stripe in $YBCO_7$ perpendicular to the *a* axis with periodicity $P_c = 4$ obtained through our all-electron fully self-consistent treatment of charge, spin, and lattice degrees of freedom. Hole doping on planar Cu and O atoms, defined as the difference in charge between the $YBCO_6$ ground state and the $YBCO_7$ stripe state (see *SI Appendix*, section 7 for details) (33–35), is indicated by changes in the relative sizes of the atoms. Directions of pink arrows denote spin orientations, and their sizes are proportional to magnetic moments. Black arrows mark directions and sizes of the major atomic displacements resulting from deformations relative to the structure of the AFM state (G-AFM) of $YBCO_7$. *C*, *Top* is a 3D rendition of the structure. Y and Ba atoms are omitted in the figure for clarity. *C*, *Middle* gives structural details in a CuO_2 plane. *C*, *Bottom* is a plot of the hole concentration on planar copper atoms and their nearest-neighbor oxygens along the *a* axis. The horizontal dashed lines mark the average experimental values obtained via NMR (33). See *SI Appendix*, section 6 for details of other stripe states. Note that both here and in *SI Appendix*, sizes of the atoms are shown schematically to highlight small differences in doping (approximately ±0.03 holes); actual doping levels are given in *C*, *Bottom* and in *SI Appendix*, Table S10. Mag., magnetic.

What is the underlying microscopic mechanism that drives the material into the stripe order through the interplay of spin, charge, and lattice degrees of freedom? The key is to recognize

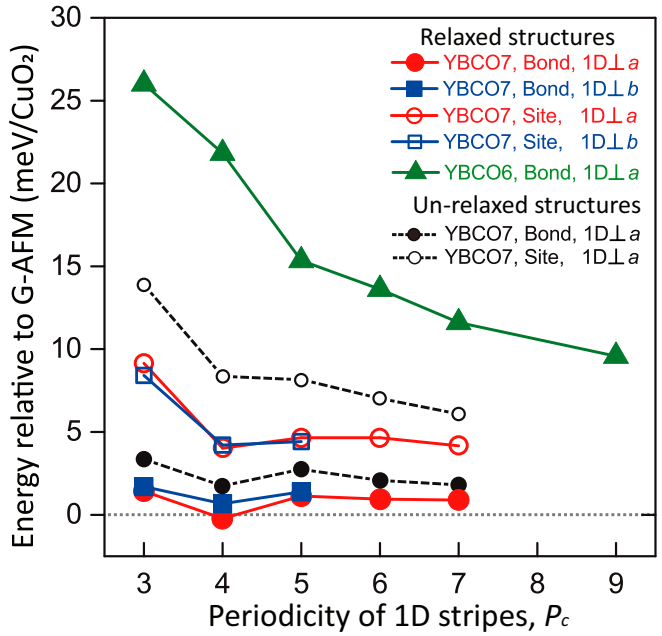

Fig. 2. Comparison of energies of various stripe states in $YBCO_6$ and $YBCO_7$. Relative energies with respect to the AFM ground state (G-AFM) as a function of the periodicity of the various 1D charge stripes (perpendicular to the *a* or *b* axis as indicated in the key) in $YBCO_7$ and $YBCO_6$ are shown. Results for 2 unrelaxed stripe structures based on the G-AFM structure are given to highlight lattice relaxation effects.

that when holes are added to the undoped system, they move to disrupt the AFM order. In reaction, there is a tendency for the holes to be expelled from the AFM domains, leaving behind magnetic stripes. The system can then be stabilized naturally by separating the magnetic stripes by APBs and the formation of charge stripes as the excess holes are accommodated in the APBs. The excess holes cause the nearby negative O ions to shift toward the positive APBs to screen them. The interaction of the lattice with spins and charges thus plays a key role in stabilizing the stripe phases. In the presence of fluctuating stripes, we would expect the formation of dynamic polarons in which a lattice distortion follows a moving electron. The strong spin–charge–lattice interplay indicated by our study suggests that phonons could play a significant role in creating the superconducting glue in the cuprates.

In comparing our results with recent studies of the 3-band (16) and 1-band (17) Hubbard models, we should keep in mind that refs. 16 and 17 neglect lattice-relaxation effects and only consider the 1/8th doping case using model dispersions appropriate for $La_{2-x}Sr_xCuO_4$, where enhanced stripe features are expected. Similar to our results, density-matrix renormalization group computations in ref. 16 found the charge modulation on oxygen to be larger than on copper; strikingly, the QMC computations of ref. 16 found that fluctuating charge modulations persist to very high temperatures. A quasidegeneracy of stripe energy vs. P_c is found in ref. 17, as is the case in our Fig. 2. However, ref. 17 found a preference for bond-centered stripes for even P_c and site-centered stripes for odd P_c, whereas our bond-centered stripes are systematically lower in energy. Also, while $P_c = 4$ is a local minimum, ref. 17 finds that the ground state corresponds to $P_c = 8$, like the trend in our results neglecting lattice relaxation. Finally, while we and ref. 16 find only weak charge modulations on the stripes, the 1-band model of ref. 17 finds unphysically large modulations (36). *SI Appendix*, sections 8 and 9 further compare the results of various approaches for treating the cuprates (14, 15, 38–44).

Fig. 2 delineates how the energies of various 1D stripe phases evolve with increasing charge periodicity, P_c, to gain insight into the nature of the anomalous normal state of the cuprates. The difference between $YBCO_6$ and $YBCO_7$ is striking. While $YBCO_7$ exhibits a multitude of low-lying competing states, in sharp contrast, $YBCO_6$ possesses a well-defined G-AFM ground state (energy 0 in the figure, dotted horizontal line) with no nearby competing states. The precursor stripes in $YBCO_6$ lie at quite high energies (filled green triangles) and are seen to be well-separated from the complex of low-energy states in $YBCO_7$. The *a*–*b* anisotropy of stripe energies that we have found gives some insight into nematicity effects, which refer to enhanced differences in properties along the *a* and *b* axis, that have been observed experimentally in many cuprates. As discussed in *SI Appendix*, section 6.2, an analysis of our results is consistent with the experimental finding that nematicity effects are stronger near optimal doping compared to the underdoped cuprates (45). In *SI Appendix*, Figs. S4–S9, we compare the bond-centered stripe of Fig. 1*C* with the site-centered and 2D stripes.

Fig. 3 compares the relative energies of 26 different states we have found in $YBCO_7$. The energy 0 is the energy of the G-AFM structure. Both 1D and 2D stripe states are considered, along with a number of uniform and nonstripe states (G-AFM, C-AFM, C′-AFM, FM, and A-AFM); details of lattice structures, energies, and other features of all these predicted states are given in *SI Appendix*, sections 4–6 (5, 46–55). Many states are nearly degenerate with the ground state, with energy differences of a few millielectronvolts (Fig. 3, *Inset*). Interestingly, a simple organizing principle emerges for the magnetic order: The red-dashed trend line shows that the stability of magnetic states increases with increasing average magnetic moment on the planar copper atoms, small-scale deviations seen in Fig. 3, *Inset* notwithstanding. In keeping with this trend, we can rule out a

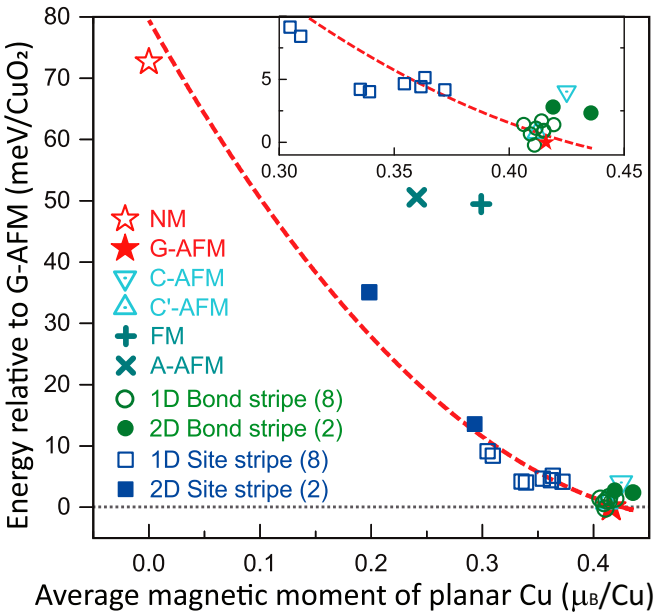

Fig. 3. Stability of the various computed stripe states in $YBCO_7$. Energies of $YBCO_7$ stripe states relative to the G-AFM structure as a function of the average magnetic moment of planar Cu atoms are shown. The dashed red line is a guide to the eye. See *SI Appendix* for details of the various structures (G-AFM, C-AFM, C′-AFM, FM, and A-AFM) presented. The integers in parentheses in the key give the total number of different structures that are shown in the figure for various types of stripes (e.g., 8 different open green circles are shown for 1D bond-type stripes). *Inset* is a blow-up of the lower right corner of the plot.

significant role of the nonmagnetic Fermi-liquid state (red unfilled star in Fig. 3) in the low-energy physics of $YBCO_7$ because the nonmagnetic state lies at a rather high energy. This result is consistent with Mott physics in the sense that a Mott insulator is characterized by restricting charge fluctuations to avoid double occupancy of orbitals and to thus promote larger local magnetic moments.

This is one of the most striking predictions of our results for $YBCO_7$, which applies to the broad spectrum of competing phases that we have uncovered. Recent resonant inelastic X-ray scattering (RIXS) experiments have found that fluctuating magnetic moments on copper atoms persist well into the overdoped regime—even in overdoped YBCO (56). Fig. 3 clearly shows that all of the low-energy phases we have found have large magnetic moments. This persistence of magnetic moments can explain the RIXS data, if we assume that RIXS sees a fluctuating average of our phases. Mook and Doğan (57) also found evidence of fluctuating stripes in $YBCO_{7-x}$ via inelastic neutron scattering, while glassy AFM order was found in LSCO throughout the pseudogap phase (58, 59). Notably, these observed stripes are predominantly 1D along the b axis, consistent with our results, and could play a significant role in driving superconductivity (57).

Our results suggest clearly that the pseudogap phase in the cuprates, represented here by $YBCO_7$, involves the presence of many competing phases and that this is the underlying mechanism through which pseudogap physics may be encoded in the material (1). An STM study of incommensurate features within the pseudogap phase finds that locally these features are composed of commensurate stripe-like patches separated by topological defects, very similar to what we are proposing here (60). Notably, an incommensurate charge-density wave (CDW) composed of commensurate stripe patches constitutes a strong-coupling CDW (61, 62), similar to McMillan's entropy-driven CDW (63). The curves of Fig. 2 can be well fit into a simple model of interacting domain walls, as discussed in *SI Appendix*, section 6.3.

Although we have discussed experimental evidence in support of our theoretical findings at various points above, we comment further here. Since static stripes have only been reported in underdoped YBCO (64), it is difficult to make direct comparisons between our predicted stripe states in $YBCO_7$ with experiments. Given that stripes are a general feature in the cuprates, however, we note that our results on YBCO are consistent with a variety of experimental observations on a number of other cuprates as follows. 1) The dominant stripe periodicity is $P_c = 4$ (65). 2) Resonant soft X-ray scattering studies (66) find stripes in LSCO-related cuprates with weak charge modulations of ± 0.031 holes and suggest that bond-centered stripes are more likely. 3) NMR studies find similar small charge modulations in many cuprates, including highly doped YBCO (67). 4) Scanning-tunneling microscopy (STM) studies find that stripes are confined in vortices and are 2D in magnetic fields with a charge modulation consistent with our results (34). Notably, our study provides a realistic material-specific basis for obtaining the value of the oxygen-to-copper hole ratio, which is a key microscopic quantity that varies systematically over the various cuprate families, and scales with the maximum superconducting T_c for each family (33, 68). While our focus here is on the stripe phases, we also find good agreement with optical and magnetic properties of the uniform magnetic phases; see *SI Appendix*, section 2.2 for details.

In conclusion, our study demonstrates how competing phases in wide classes of complex quantum materials can be addressed on a first-principles basis without the need to invoke ad hoc parameters or to restrict the orbitals included in the underlying Hamiltonian. Our finding that energy minimization is controlled by maximizing the Cu local moment shows that Mott physics continues to play a significant role in $YBCO_7$ and that this physics can be captured effectively within our first-principles framework. Our approach will thus deepen understanding of the fascinating exotic properties of quantum materials and how these properties emerge through the interplay of spin, charge, and lattice degrees of freedom.

Computational Details

All calculations were carried out by using the Vienna Ab-initio Simulation Package (69–71) with the SCAN exchange-correlation functional (18). A relatively high cutoff of energy of 500 eV was used to truncate the plane-wave basis set. *SI Appendix*, section 10 discusses issues related to the convergence of the results with respect to the energy of the plane-wave cutoff and the density of the k mesh; the specific k meshes employed in computations are also given. Spin-orbit coupling effects were neglected in the schematics of Fig. 1, where the spins are shown as vertical arrows for simplicity. For the uniform magnetic phases, spin-orbit coupling caused the spins to lie mostly in-plane (*SI Appendix*, sections 4 and 5), which is consistent with experimental findings and our calculations on $La_{2-x}Sr_xCuO_4$ (13). All crystal structures were fully relaxed with a force-convergence criterion of 0.01 eV/Å, unless specified otherwise. In order to stabilize a stripe, we only constrained the supercell shape and gave an initial guess for the spin configuration, but otherwise, all degrees of freedom (charge, spin, and lattice) were relaxed simultaneously until full self-consistency was achieved and the state of minimum energy was found. To determine the average hole doping in each state, the Bader charge analysis (72, 73) was employed (*SI Appendix*, section 7).

Data and Materials Availability. All relevant data are provided in the main text and/or *SI Appendix*.

ACKNOWLEDGMENTS. We thank Hoang Tran, Carl Baribault, and Hideki Fujioka for their computational support at Tulane University. The work at Tulane University was supported by start-up funding from Tulane University, the Cypress Computational Cluster at Tulane, the Department of Energy (DOE) Energy Frontier Research Centers (development and applications of DFT): Center for Complex Materials from First Principles Grant DE-SC0012575, the DOE, Office of Science, Basic Energy Sciences Grant DE-SC0019350 (core research), and the National Energy Research Scientific Computing Center supercomputing center. The work at Northeastern University was supported by the DOE, Office of Science, Basic Energy Sciences Grant DE-FG02-07ER46352 (core research) and benefited from Northeastern University's Advanced Scientific Computation Center, the National Energy Research Scientific Computing Center supercomputing center (DOE Grant DEAC02-05CH11231), and support (testing the efficacy of new functionals in diversely bonded materials) from the DOE Energy Frontier Research Center: Center for Complex Materials from First Principles Grant DE-SC0012575. The work at Temple University was also supported by NSF Grant DMR-1607868 (Condensed Matter and Materials Theory Program, Division of Materials Research, with a contribution from Chemical Theory, Models, and Computational Methods–Division of Chemistry). B.B. acknowledges support from the COST Action CA16218.

1. E. Fradkin, S. A. Kivelson, J. M. Tranquada, Theory of intertwined orders in high temperature superconductors. *Rev. Mod. Phys.* **87**, 457–482 (2015).
2. J. M. Tranquada, B. J. Sternlieb, J. D. Axe, Y. Nakamura, S. Uchida, Evidence for stripe correlations of spins and holes in copper oxide superconductors. *Nature* **375**, 561–563 (1995).
3. S. R. White, D. J. Scalapino, Density matrix renormalization group study of the striped phase in the 2D t–J Model. *Phys. Rev. Lett.* **80**, 1272–1275 (1998).
4. S. A. Kivelson *et al.*, How to detect fluctuating stripes in the high-temperature superconductors. *Rev. Mod. Phys.* **75**, 1201–1241 (2003).
5. J. R. Schrieffer, Ed., *Handbook of High-Temperature Superconductivity: Theory and Experiment* (Springer, New York, 2007).
6. I. M. Vishik, Photoemission perspective on pseudogap, superconducting fluctuations, and charge order in cuprates: A review of recent progress. *Rep. Prog. Phys.* **81**, 062501 (2018).
7. B. G. Levi, Are stripes a universal feature of high-T_c superconductors? *Phys. Today* **51**, 19–22 (1998).
8. I. M. Vishik *et al.*, Phase competition in trisected superconducting dome. *Proc. Natl. Acad. Sci. U.S.A.* **109**, 18332–18337 (2012).
9. R. M. Fernandes, P. P. Orth, J. Schmalian, Intertwined vestigial order in quantum materials: Nematicity and beyond. *Annu. Rev. Condens. Matter Phys.* **10**, 133–154 (2019).

10. J. Bertinshaw, Y. K. Kim, G. Khaliullin, B. J. Kim, Square lattice iridates. *Annu. Rev. Condens. Matter Phys.* **10**, 315–336 (2019).
11. J. K. Glasbrenner *et al*., Effect of magnetic frustration on nematicity and superconductivity in iron chalcogenides. *Nat. Phys.* **11**, 953–958 (2015).
12. J. W. Furness *et al*., An accurate first-principles treatment of doping-dependent electronic structure of high-temperature cuprate superconductors. *Commun. Phys.* **1**, 11 (2018).
13. C. Lane *et al*., Antiferromagnetic ground state of La_2CuO_4: A parameter-free ab initio description. *Phys. Rev. B* **98**, 125140 (2018).
14. V. I. Anisimov *et al*., Computation of stripes in cuprates within the LDA+U method. *Phys. Rev. B Condens. Matter Mater. Phys.* **70**, 172501 (2004).
15. S. Pesant, M. Côté, DFT + U study of magnetic order in doped La_2CuO_4 crystals. *Phys. Rev. B Condens. Matter Mater. Phys.* **84**, 085104 (2011).
16. E. W. Huang *et al*., Numerical evidence of fluctuating stripes in the normal state of high-T_c cuprate superconductors. *Science* **358**, 1161–1164 (2017).
17. B.-X. Zheng *et al*., Stripe order in the underdoped region of the two-dimensional Hubbard model. *Science* **358**, 1155–1160 (2017).
18. J. Sun, A. Ruzsinszky, J. P. Perdew, Strongly constrained and appropriately normed semilocal density functional. *Phys. Rev. Lett.* **115**, 036402 (2015).
19. J. Sun *et al*., Accurate first-principles structures and energies of diversely bonded systems from an efficient density functional. *Nat. Chem.* **8**, 831–836 (2016).
20. A. Paul, J. Sun, J. P. Perdew, U. V. Waghmare, Accuracy of first-principles interatomic interactions and predictions of ferroelectric phase transitions in perovskite oxides: Energy functional and effective Hamiltonian. *Phys. Rev. B* **95**, 054111 (2017).
21. Y. Zhang, J. Sun, J. P. Perdew, X. Wu, Comparative first-principles studies of prototypical ferroelectric materials by LDA, GGA, and SCAN meta-GGA. *Phys. Rev. B* **96**, 035143 (2017).
22. M. Chen *et al*., *Ab initio* theory and modeling of water. *Proc. Natl. Acad. Sci. U.S.A.* **114**, 10846–10851 (2017).
23. A. Patra, J. E. Bates, J. Sun, J. P. Perdew, Properties of real metallic surfaces: Effects of density functional semilocality and van der Waals nonlocality. *Proc. Natl. Acad. Sci. U.S.A.* **114**, E9188–E9196 (2017).
24. Y. Zhang *et al*., Efficient first-principles prediction of solid stability: Towards chemical accuracy. *Npj Computational Materials* **4**, 9 (2018).
25. S. Uchida *et al*., Optical spectra of $La_{2-x}Sr_xCuO_4$: Effect of carrier doping on the electronic structure of the CuO_2 plane. *Phys. Rev. B Condens. Matter* **43**, 7942–7954 (1991).
26. S. Ono, S. Komiya, Y. Ando, Strong charge fluctuations manifested in the high-temperature hall coefficient of high-T_c cuprates. *Phys. Rev. B Condens. Matter Mater. Phys.* **75**, 024515 (2007).
27. T. Das, R. S. Markiewicz, A. Bansil, Optical model-solution to the competition between a pseudogap phase and a charge-transfer-gap phase in high-temperature cuprate superconductors. *Phys. Rev. B Condens. Matter Mater. Phys.* **81**, 174504 (2010).
28. C. Ye *et al*., Visualizing the atomic-scale electronic structure of the $Ca_2CuO_2Cl_2$ Mott insulator. *Nat. Commun.* **4**, 1365 (2013).
29. M. A. Kastner, R. J. Birgeneau, G. Shirane, Y. Endoh, Magnetic, transport, and optical properties of monolayer copper oxides. *Rev. Mod. Phys.* **70**, 897–928 (1998).
30. J. P. Perdew *et al*., Understanding band gaps of solids in generalized Kohn-Sham theory. *Proc. Natl. Acad. Sci. U.S.A.* **114**, 2801–2806 (2017).
31. R. Comin, A. Damascelli, Resonant X-ray scattering studies of charge order in cuprates. *Annu. Rev. Condens. Matter Phys.* **7**, 369–405 (2016).
32. R. Comin *et al*., Symmetry of charge order in cuprates. *Nat. Mater.* **14**, 796–800 (2015).
33. J. Haase, O. P. Sushkov, P. Horsch, G. V. M. Williams, Planar Cu and O hole densities in high-T_c cuprates determined with NMR. *Phys. Rev. B Condens. Matter Mater. Phys.* **69**, 094504 (2004).
34. J. E. Hoffman *et al*., A four unit cell periodic pattern of quasi-particle states surrounding vortex cores in $Bi_2Sr_2CaCu_2O_{8+\delta}$. *Science* **295**, 466–469 (2002).
35. H. Eskes, M. B. J. Meinders, G. A. Sawatzky, Anomalous transfer of spectral weight in doped strongly correlated systems. *Phys. Rev. Lett.* **67**, 1035–1038 (1991).
36. W. Luo *et al*., Orbital-occupancy versus charge ordering and the strength of electron correlations in electron-doped $CaMnO_3$. *Phys. Rev. Lett.* **99**, 036402 (2007).
37. T. Niemöller *et al*., Charge stripes seen with X-rays in $La_{1.45}Nd_{0.4}Sr_{0.15}CuO_4$. *Eur. Phys. J. B* **12**, 509–513 (1999).
38. J. K. Perry, J. Tahir-Kheli, W. A. Goddard, Antiferromagnetic band structure of La_2CuO_4: Becke-3–Lee-Yang-Parr calculations. *Phys. Rev. B Condens. Matter Mater. Phys.* **63**, 144510 (2001).
39. C. H. Patterson, Small polarons and magnetic antiphase boundaries in $Ca_{2-x}Na_xCuO_2Cl_2$ (x = 0.06,0.12): Origin of striped phases in cuprates. *Phys. Rev. B Condens. Matter Mater. Phys.* **77**, 094523 (2008).
40. Ide. P. Moreira, P. Rivero, F. Illas, Electronic structure of $HgBa_2Ca_{(n-1)}Cu_{(n)}O_{(2n+2)}$ (n = 1, 2, 3) superconductor parent compounds from periodic hybrid density functional theory. *J. Chem. Phys.* **134**, 074709 (2011).
41. L. Hozoi, S. Nishimoto, G. Kalosakas, D. B. Bodea, S. Burdin, Nonlocal interactions in doped cuprates: Correlated motion of Zhang-Rice polarons. *Phys. Rev. B Condens. Matter Mater. Phys.* **75**, 024517 (2007).
42. K. Foyevtsova *et al*., Ab initio quantum Monte Carlo calculations of spin superexchange in cuprates: The benchmarking case of Ca_2CuO_3. *Phys. Rev. X* **4**, 031003 (2014).
43. L. K. Wagner, P. Abbamonte, Effect of electron correlation on the electronic structure and spin-lattice coupling of high-T_c cuprates: Quantum Monte Carlo calculations. *Phys. Rev. B Condens. Matter Mater. Phys.* **90**, 125129 (2014).
44. L. K. Wagner, Ground state of doped cuprates from first-principles quantum Monte Carlo calculations. *Phys. Rev. B Condens. Matter Mater. Phys.* **92**, 161116 (2015).
45. C. V. Parker *et al*., Fluctuating stripes at the onset of the pseudogap in the high-T(c) superconductor $Bi_{(2)}Sr_{(2)}CaCu_{(2)}O_{(8+x)}$. *Nature* **468**, 677–680 (2010).
46. P. Burlet, J. Y. Henry, L. P. Regnault, In-plane magnetic anisotropy in antiferromagnetic $YBa_2Cu_3O_{6+x}$. *Physica C* **296**, 205–209 (1998).
47. A. Jánossy *et al*., Antiferromagnetic domains in $YBa_2Cu_3O_{6+x}$ probed by Gd^{3+} ESR. *Phys. Rev. B Condens. Matter Mater. Phys.* **59**, 1176–1184 (1999).
48. H. Yasuoka, T. Shimizu, Y. Ueda, K. Kosuge. Observation of antiferromagnetic nuclear resonance of Cu in $YBa_2Cu_3O_6$. *J. Phys. Soc. Jpn.* **57**, 2659–2662 (1988).
49. J. Rossat-Mignod, P. Burlet, M. J. G. M. Jurgens, J. Y. Henry, C. Vettier, Evidence for high temperature antiferromagnetic ordering in $YBa_2Cu_3O_6$. *Physica C Supercond.* **152**, 19–24 (1988).
50. P. Mendels, H. Alloul, Zero field NMR of the magnetic copper sites in antiferromagnetic $YBa_2Cu_3O_{6+x}$. *Physica C Supercond.* **156**, 355–358 (1988).
51. J. M. Tranquada *et al*., Neutron-diffraction determination of antiferromagnetic structure of Cu ions in YBa2Cu. *Phys. Rev. Lett.* **60**, 156–159 (1988).
52. J. Rossat-Mignod *et al*., Investigation of the spin dynamics in $YBa_2Cu_3O_{6+x}$ by inelastic neutron scattering. *Physica B Condens. Matter* **169**, 58–65 (1991).
53. J. Rossat-Mignod, Antiferromagnetic ordering and phase diagram of $YBa_2Cu_3O_{6+x}$. *J. Phys. Colloq.* **49**, 2119–2124 (1988).
54. S. Shamoto, M. Sato, J. M. Tranquada, B. J. Sternlieb, G. Shirane, Neutron-scattering study of antiferromagnetism in $YBa_2Cu_3O_{6.15}$. *Phys. Rev. B Condens. Matter* **48**, 13817–13825 (1993).
55. R. S. Markiewicz, STM checkerboards from crossed stripes: A static stripe model. *Phys. Rev. B Condens. Matter Mater. Phys.* **71**, 220504 (2005).
56. M. L. Tacon *et al*., Intense paramagnon excitations in a large family of high-temperature superconductors. *Nat. Phys.* **7**, 725–730 (2011).
57. H. A. Mook, F. Doğan, Charge fluctuations in $YBa_2Cu_3O_{7-x}$ high-temperature superconductors. *Nature* **401**, 145–148 (1999).
58. M. Frachet *et al*., Hidden magnetism at the pseudogap critical point of a high temperature superconductor. arXiv:1909.10258 (23 September 2019).
59. R. J. Birgeneau *et al*., Antiferromangetic spin correlations in insulating, metallic, and superconducting La2-xSrx. *Phys. Rev. B Condens. Matter* **38**, 6614–6623 (1988).
60. A. Mesaros *et al*., Topological defects coupling smectic modulations to intra-unit-cell nematicity in cuprates. *Science* **333**, 426–430 (2011).
61. X. Zhu, J. Guo, J. Zhang, E. W. Plummer, Misconceptions associated with the origin of charge density waves. *Adv. Phys. X* **2**, 622–640 (2017).
62. X. Zhu, Y. Cao, J. Zhang, E. W. Plummer, J. Guo, Classification of charge density waves based on their nature. *Proc. Natl. Acad. Sci. U.S.A.* **112**, 2367–2371 (2015).
63. W. L. McMillan, Microscopic model of charge-density waves in 2H–$TaSe_2$. *Phys. Rev. B* **16**, 643–650 (1977).
64. H. A. Mook, P. Dai, F. Doğan, Charge and spin structure in of YBa(2)Cu(3)O(6.35). *Phys. Rev. Lett.* **88**, 097004 (2002).
65. T. A. Webb *et al*., Density wave probes cuprate quantum phase transition. *Phys. Rev. X* **9**, 021021 (2019).
66. P. Abbamonte, E. Demler, J. C. Séamus Davis, J.-C. Campuzano, Stripes and electronic liquid crystals in strongly correlated materials. *Physica C* **481**, 15–22 (2012).
67. M. Jurkutat, A. Erb, J. Haase, T_c and other cuprate properties in relation to planar charges as measured by NMR. *Condens. Matter* **4**, 67 (2019).
68. D. Rybicki, M. Jurkutat, S. Reichardt, C. Kapusta, J. Haase, Perspective on the phase diagram of cuprate high-temperature superconductors. *Nat. Commun.* **7**, 11413 (2016).
69. P. E. Blöchl, Projector augmented-wave method. *Phys. Rev. B Condens. Matter* **50**, 17953–17979 (1994).
70. G. Kresse, J. Furthmüller, Efficient iterative schemes for *ab initio* total-energy calculations using a plane-wave basis set. *Phys. Rev. B Condens. Matter* **54**, 11169–11186 (1996).
71. G. Kresse, D. Joubert, From ultrasoft pseudopotentials to the projector augmented-wave method. *Phys. Rev. B Condens. Matter Mater. Phys.* **59**, 1758–1775 (1999).
72. R. F. W. Bader, *Atoms in Molecules: A Quantum Theory* (International Series of Monographs on Chemistry, Oxford University Press, Oxford, UK, 1994), vol. 22.
73. W. Tang, E. Sanville, G. Henkelman, A grid-based Bader analysis algorithm without lattice bias. *J. Phys. Condens. Matter* **21**, 084204 (2009).